JACS
JOURNAL OF THE AMERICAN CHEMICAL SOCIETY

COMMUNICATION

pubs.acs.org/JACS

Cathodic Corrosion as a Facile and Effective Method To Prepare Clean Metal Alloy Nanoparticles

Paramaconi Rodriguez,*[,†] Frans D. Tichelaar,[‡] Marc T. M. Koper,[†] and Alexei I. Yanson*[,†]

[†]Leiden Institute of Chemistry, Leiden University, Postbus 9502, 2300 RA Leiden, The Netherlands

[‡]Kavli Institute of NanoScience, Delft University of Technology, Lorentzweg 1, 2628 CJ Delft, The Netherlands

Supporting Information

ABSTRACT: The cathodic corrosion method described here is a simple, clean, and fast way of synthesizing nanoalloys with high catalytic performance. Using a series of Pt−Rh alloys as an example, we show that this one-step method can convert a bulk alloy electrode into an aqueous suspension of nanoparticles, retaining the composition and crystal lattice structure of the starting alloy. Compared to pure metals, these alloy nanocatalysts are more active toward CO and methanol oxidation and nitrate reduction reactions. Nanoparticles made of PtRu, PtIr, PtNi, AuCo, AuCu, and FeCo bulk alloys demonstrate the universality of this synthesis method.

Ever since the Bronze Age, humankind's progress has been facilitated by the use of alloys, and today alloys are used everywhere from cutlery to turbines. Heterogeneous catalysis is a field in which the use of alloy nanoparticles is important for producing more cost-efficient, more active, and more selective catalysts.[1,2] While the technology for the fabrication of bulk metal alloys has been perfected over centuries, until now there has been no universal method to rapidly synthesize metal alloy nanoparticles with predefined composition, structure, and catalytic properties. In this Communication we report on a conceptually novel method for making alloy nanoparticles by cathodic atomization of bulk alloys. We show that the composition of the nanoparticles is essentially identical to that of the starting alloy material, while their catalytic properties match or exceed those of similar alloy catalysts prepared by colloidal methods.

Most methods of chemical synthesis of alloy and core−shell nanoparticles involve (co)reduction of metal salts within micelles or colloids,[3−6] while the so-called carbonyl synthesis route offers an intriguing variation by creating a bimetallic precursor.[6,7] While much work has been done to perfect these methods for making nanoparticles, they present inherent inconveniences. First is the inevitable presence of the organic components employed during the synthesis on the surface of the nanoparticles, which is also applicable to pure metal nanoparticles. These surfactants or capping materials contaminate the final product and adversely affect its performance, e.g., in catalysis[8−13] or in biological applications.[14,15] Gas-phase synthesis, like laser vaporization of solid targets, magnetron sputtering, or ion sputtering, gives clean nanoparticles, including alloys and mixtures, but the technique suffers from low yields and the relatively wide size distribution and particle agglomeration.[16,17] The impregnation and incipient wetness method of supported nanoparticles synthesis often results in relatively large particles with a nonuniform composition due to support irregularities and segregation of metals due to the differences in their reducibility.[12,18]

Recently, a radically different method of nanoparticles synthesis has been developed that avoids many of these shortcomings.[19,20] This method, which works for a wide variety of metals, proceeds via cathodic corrosion of a metal electrode, rapidly atomizing it into a suspension of metal nanoparticles. By using this method one can synthesize small, clean, and catalytically active nanoparticles that are directly usable as catalysts. Our current understanding of this process is that, at the strongly negative electrode potentials employed, highly nonequilibrium (clusters of) negative metal anions are formed, which serve as precursors for the formation of the nanostructures and nanoparticles.[19] Because of the nonequilibrium conditions, we propose that, instead of going through the preferential dissolution of one of the metals, the reaction goes through the dissolution of negatively charged alloy clusters. Here we demonstrate that this method can also be used for the synthesis of metal alloy nanoparticles. Using a series of Pt_xRh_y wires, we verify the ability of the method to retain alloy composition from bulk metal to nanoparticles. We also present evidence that the method works for other commercially available as well as custom metal alloys, demonstrating a high degree of universality while maintaining good control of alloy composition.

The experimental setup is presented in Figure 1A. In brief, an alloy wire to be atomized is immersed in an electrolyte, and ac potential versus a glassy carbon counter electrode is applied until all submerged metal is converted into a black suspension of metal nanoparticles. A negative dc offset ensures that the formation of the nanoparticles proceeds via a reduction (cathodic) process.[19] The average currents during each negative (positive) voltage half-cycle are plotted as a function of time as shown in Figure 1D. The initial saturation of the current is due to limited capacity for hydrogen gas evolution, while the decrease of the current toward the end is due to the corrosion of the wire. The positive currents at the non-negative voltage half-cycle (0 V) are related to the oxidation of the hydrogen formed at the negative cycle. A black suspension coming off the electrode can be observed throughout the experiment. As can be seen in Figure 1, a wire of ca. 0.12 mm diameter, immersed 2.5 mm in the solution, can be dispersed into nanoparticles in around 500 s.[21]

Received: September 10, 2011
Published: October 07, 2011

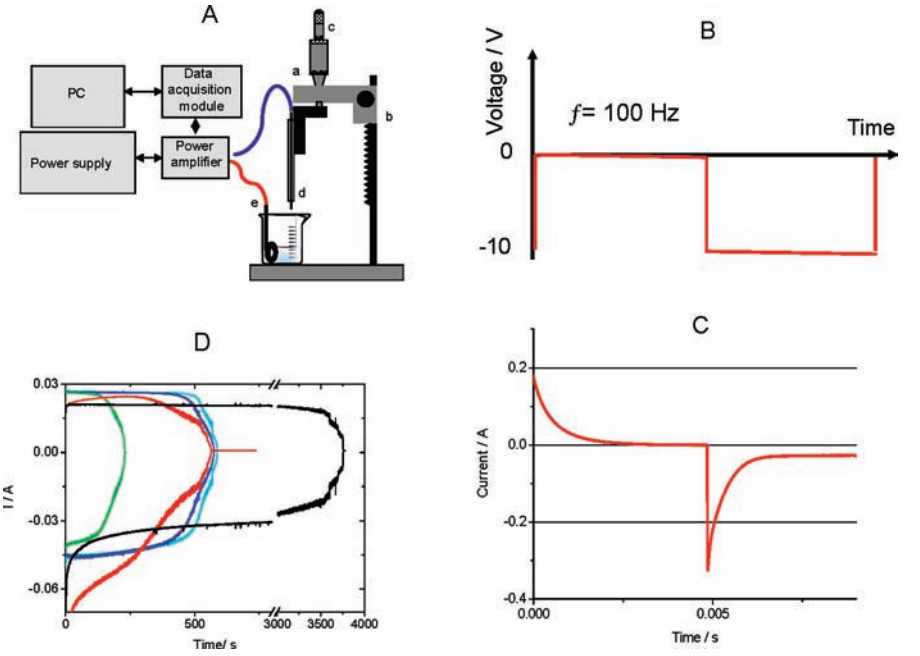

Figure 1. (A) Experimental setup for the cathodic corrosion synthesis of the nanoparticles: (a) support, (b) coarse screw, (c) fine micrometric screw, (d) working electrode, and (e) high surface area electrode. (B) Potential program applied: square wave between 0 and −10 V and 100 Hz. (C) Current responses at the electrode at 100 s for the $Pt_{70}Rh_{30}$ wire. (D) Average ac current measured during the positive (negative) half-cycle vs time for different PtRh wires: (light blue) Pt, (dark blue) $Pt_{90}Rh_{10}$, (green) $Pt_{70}Rh_{30}$, (red) $Pt_{20}Rh_{80}$, and (black) Rh. The wire was always submerged 2.5 mm into the solution. Test solution: 1 M NaOH. $E_{appl} = \pm 5$ V, offset = −5 V, $f = 100$ Hz.

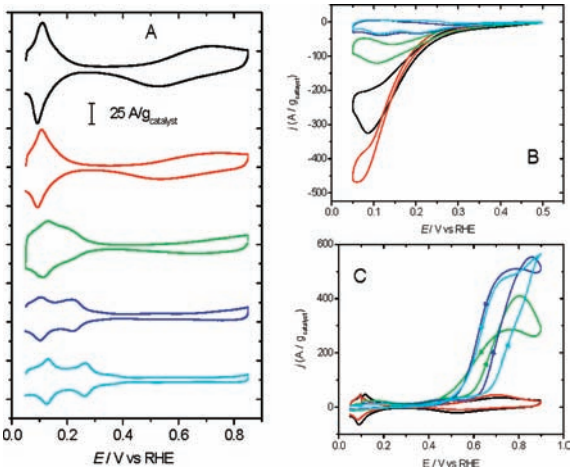

Figure 2. Voltammetric profiles for (light blue) Pt, (dark blue) $Pt_{90}Rh_{10}$, (green) $Pt_{70}Rh_{30}$, (red) $Pt_{20}Rh_{80}$, and (black) Rh nanoparticles supported on a gold polycrystalline disk in (A) 0.5 M H_2SO_4 (B) 0.5 M H_2SO_4 + 0.01 M $NaNO_3$ solution, and (C) 0.5 M H_2SO_4 + 0.5 M CH_3OH solution. Scan rate: (A) 50 and (B,C) 20 mV/s.

Next we studied the electrochemical properties of the nanoparticles prepared by the cathodic corrosion method. In the case of platinum and some related metals, recording a current−voltage characteristic of an electrochemical interface under controlled conditions (a so-called blank voltammogram) is a well-established method to determine qualitatively not only the composition of the electrode material but also the cleanliness of the interface.[10,25−27] Figure 2A shows the blank voltammetry of the PtRh nanoparticles supported on a gold electrode in sulfuric acid. The features between 0.05 and 0.4 V are related to the adsorption/desorption of a monolayer of hydrogen and anions,[28] and those between 0.4 and 0.9 V to the adsorption/desorption of OH species on Rh.[29,30] The voltammetric profiles of Pt and Rh nanoparticles are in good agreement with previous results obtained for polycrystalline electrodes in the same solution.[29,30] By calculating the charge under the hydrogen desorption/adsorption peaks, and knowing the mass of the catalyst, we can estimate the average size of the nanoparticles for pure metals. The values (Pt ≈ 9 nm and Rh ≈ 6 nm) obtained by this approximation agree with those obtained by TEM and XRD (Figure 3A,C).

The blank voltammograms present two characteristics indicative of bimetallic nanoparticles. As the content of Rh is increased, at the lower potentials the two peaks of hydrogen shift toward more negative potentials, becoming one single peak characteristic of Rh. In the higher potential region, the charge related to the adsorption/desorption of OH increases with the concentration of Rh in the sample.[29,30]

Having characterized the nanoparticles synthesized by this method, we studied the activity of these nanoparticles toward three important electrocatalytic reactions: nitrate reduction, CO oxidation, and methanol oxidation. The oxidation of methanol on bimetallic catalysts is an important and widely studied reaction due to applications in low-temperature fuel cells, with a number of studies on PtRh alloys.[31−33] As for the reduction of nitrate, Rh is generally considered to be most active monometallic electrocatalyst,[34,35] but remarkably little attention has been given to PtRh alloys for this reaction.[36]

Figure 2B shows the voltammograms of nitrate reduction in acidic solution over PtRh alloy nanocatalysts. Two important behaviors should be highlighted:

The maximum negative current, corresponding to the reduction of nitrate, increases proportionally to the content of Rh, but

dx.doi.org/10.1021/ja208264e |J. Am. Chem. Soc. 2011, 133, 17626–17629

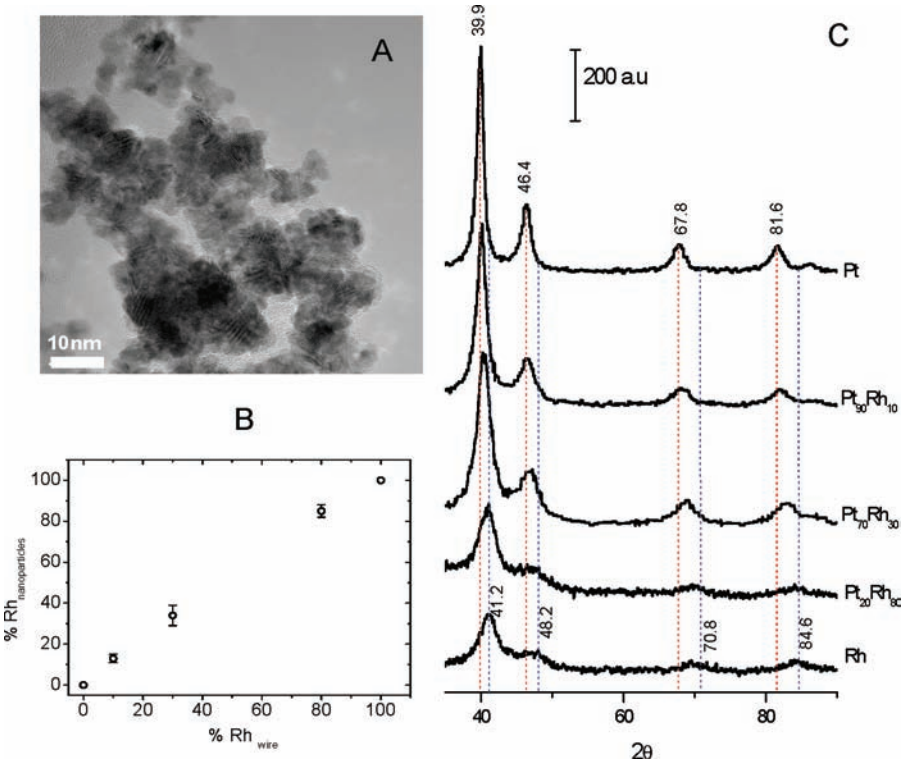

Figure 3. (A) TEM image of the $Pt_{90}Rh_{10}$ nanoparticles sample. (B) Rh content in the nanoparticles sample obtained from EDX spectra as a function of the content of Rh on the wire (commercial data). (C) XRD patterns of nanoparticles with different Pt_xRh.

surprisingly the $Rh_{80}Pt_{20}$ nanoalloy exhibits an even higher current density than pure Rh nanoparticles, also when compared in terms of current density per electrochemically active surface area. The maximun current density observed in the sample $Rh_{80}Pt_{20}$ is 560 $\mu A/cm^2$, while the maximum current density observed in the pure Rh sample for the same concentration for nitrate is 400 $\mu A/cm^2$. Previous results for Rh nanoparticles [20] and Rh massive electrode[34] report maximum currents of 500 $\mu A/cm^2$ (in a 10 times more concentrated solution) and 300 $\mu A/cm^2$.

The $Rh_{80}Pt_{20}$ sample also exhibits a smaller difference between the reduction currents in the negative and positive scans, suggesting that the reactivity of intermediate species (nitrite, NO) leads to less hysteresis compared to the other samples. While Rh is generally considered the best monometallic catalyst for nitrate reduction,[34] the observation that our $Rh_{80}Pt_{20}$ nanoparticles are superior to pure Rh is new and significant. The high activity of Rh is usually ascribed to its ability to strongly bind (oxy)anions. Further studies would be required to elucidate the origin of the enhanced activity of the $Rh_{80}Pt_{20}$ nanoparticles.

Figure 2C shows the voltammetric response of the supported nanoparticles toward the oxidation of methanol. As can be seen, the samples of Rh and $Rh_{80}Pt_{20}$ show no (or negligible) activity toward the oxidation of methanol, in agreement with previous results on bulk electrodes.[31−33] This is due to the inhibition of methanol adsorption by the strong adsorption of poisoning CO on Rh, as reported earlier.[32] The samples with higher platinum content, however, show significant oxidation currents in the potential region between 0.4 and 0.9 V. The voltammetric profiles of the three high-content platinum samples show very similar behavior, the most important characteristic being the hysteresis between the positive and negative scans. The lower oxidation currents during the positive scan are due to the initial CO poisoning of the surface. At higher potentials this CO is oxidized off the surface, and during the negative scan the oxidation of methanol is not limited by the presence or formation of the poison, and for that reason the currents are higher.

The alloys $Pt_{90}Rh_{10}$ and $Pt_{70}Rh_{30}$ present a hysteresis of about 60 mV between the positive and negative scans, which is 40 mV smaller than the hysteresis of the Pt sample. This is probably due to the higher reactivity of these alloys toward the oxidation of surface-poisoning CO (see also Figure S5). It is therefore clear that, compared to pure metals, PtRh alloys show better catalytic activity for the oxidation of methanol and CO, which are reactions of special interest for fuel cells and, in the gas phase, for automotive exhaust catalysis.[13,13,31,32]

To demonstrate the universality of our cathodic atomization method, we have prepared nanoparticles from $Pt_{80}Ir_{20}$, $Pt_{95}Ru_5$, and $Pt_{50}Ni_{50}$ alloy wires, and also AuCo, AuCu, and FeCo alloys. In all cases TEM analysis shows nanoparticles with a mean size below 10 nm, EDX confirms the bimetallic composition, and the shift of XRD lines indicates proper alloying.[23] Electrochemical studies of CO and methanol oxidation on PtRu nanoalloys, and the oxygen reduction reaction on PtNi nanoalloys, as prepared by the method of cathodic corrosion, confirm their usability as nanocatalysts.[23]

To summarize, we have shown that cathodic corrosion is a facile method to prepare clean nanoparticles of various alloys that can be used directly as (electro)catalysts. We demonstrate that these nanoparticles are properly alloyed and retain the composition of the starting bulk material. For the PtRh alloys, the size decreases as a function of Rh content: we obtained Rh nanoparticles of 4 ± 2 nm and alloy nanoparticles of 5 ± 3 nm. Even smaller nanoparticles were obtained for PtRu (3 ± 3 nm), which also showed excellent catalytic properties toward CO and methanol

oxidation. While we have tested this method for binary alloys, it is to be expected that the method should also work for ternary alloys, thereby further expanding the range of applications. Moreover, their catalytic properties can be tuned further by subsequent annealing and/or chemical etching treatments, for instance toward the preparation of core−shell or de-alloyed nanoparticles[2,37−40]

■ ASSOCIATED CONTENT

Supporting Information. Further experimental details and characterization of the nanoparticles. This material is available free of charge via the Internet at http://pubs.acs.org.

■ AUTHOR INFORMATION

Corresponding Author
rodriguezperezpb@chem.leidenuniv.nl; a.yanson@chem.leidenuniv.nl

■ ACKNOWLEDGMENT

We thank T. H. Oosterkamp for providing generous access to the SEM facility. P.R., A.I.Y., and M.T.M.K. acknowledge financial support from The Netherlands Organization for Scientific Research (NWO) through VENI, VIDI, and VICI grants, respectively.

■ REFERENCES

(1) Greeley, J.; Jaramillo, T. F.; Bonde, J.; Chorkendorff, I. B.; Norskov, J. K. *Nat. Mater.* **2006**, *5*, 909–913.
(2) Greeley, J.; Mavrikakis, M. *Nat. Mater.* **2004**, *3*, 810–815.
(3) Alayoglu, S.; Nilekar, A. U.; Mavrikakis, M.; Eichhorn, B. *Nat. Mater.* **2008**, *7*, 333–338.
(4) Wu, J.; Gross, A.; Yang, H. *Nano Lett.* **2011**, *11*, 798–802.
(5) Mallin, M. P.; Murphy, C. J. *Nano Lett.* **2002**, *2*, 1235–1237.
(6) Favry, E.; Wang, D.; Fantauzzi, D.; Anton, J.; Su, D. S.; Jacob, T.; Alonso-Vante, N. *Phys. Chem. Chem. Phys.* **2011**, *13*, 9201–9208.
(7) Yang, H.; Vogel, W.; Lamy, C.; Alonso-Vante, N. *J. Phys. Chem. B* **2004**, *108*, 11024–11034.
(8) Hirai, H. *J. Macromol. Sci. Chem.* **1979**, *13*, 633−649.
(9) Solla-Gullon, J.; Montiel, V.; Aldaz, A.; Clavilier, J. *J. Electroanal. Chem.* **2000**, *491*, 69–77.
(10) Solla-Gullon, J.; Montiel, V.; Aldaz, A.; Clavilier, J. *J. Electrochem. Soc.* **2003**, *150*, E104–E109.
(11) Bratlie, K. M.; Lee, H.; Komvopoulos, K.; Yang, P.; Somorjai, G. A. *Nano Lett.* **2007**, *7*, 3097–3101.
(12) Zhou, B.; Hermans, S.; Somorjai, G. A. *Nanotechnology in Catalysis*; Kluwer Academic/Plenum Publishers: New York, 2011.
(13) Park, J. Y.; Zhang, Y.; Grass, M.; Zhang, T.; Somorjai, G. A. *Nano Lett.* **2008**, *8*, 673–677.
(14) Niidome, T.; Yamagata, M.; Okamoto, Y.; Akiyama, Y.; Takahashi, H.; Kawano, T.; Katayama, Y.; Niidome, Y. *J. Controlled Release* **2006**, *114*, 343–347.
(15) Connor, E.; Mwamuka, J.; Gole, A.; Murphy, C.; Wyatt, M. *Small* **2005**, *1*, 325–327.
(16) Kruis, F. E.; Fissan, H.; Peled, A. *J. Aerosol Sci.* **1998**, *29*, 511–535.
(17) Milani, P.; Iannotta, I. *Cluster beam synthesis of nanostructured materials*; Springer: Berlin, 1999.
(18) Robertson, S. D.; McNicol, B. D.; De Baas, J. H.; Kloet, S. C.; Jenkins, J. W. *J. Catal.* **1975**, *37*, 424–431.
(19) Yanson, A. I.; Rodriguez, P.; Garcia-Araez, N.; Mom, R. V.; Tichelaar, F. D.; Koper, M. T. M. *Angew. Chem., Int. Ed.* **2011**, *50*, 6346–6350.
(20) Liu, J.; Huang, W.; Chen, S.; Hu, S.; Liu, F.; Li, Z. *Int. J. Electrochem. Sci.* **2009**, *4*, 1302–1308.
(21) Similar etching times were found for the wires with 80% and 10% Rh. For the wire with 30% Rh, the etching time is half, and for 100% Rh it is 10 times more. This is not related to an experimental error, as shown in Supporting Information (Figure S1). The differences in the etching times of the alloys could be due to variations in the microscopic structure of the alloys induced by wire drawing.
(22) Jenkins, R.; Snyder, R. *Introduction to X-Ray powder diffractometry*; John Wiley and Sons Inc.: New York, 1996.
(23) See Supporting Information.
(24) Park, K. W.; Han, D. S.; Sung, Y. E. *J. Power Sources* **2006**, *163*, 82–86.
(25) Clavilier, J.; El Achi, K.; Petit, M.; Rodes, A.; Zamakhchari, M. A. *J. Electroanal. Chem.* **1990**, *295*, 333.
(26) Bard, A. J.; Faulkner, L. R. *Electrochemical Methods. Fundamentals and Applications*; John Wiley & Sons: New York, 1980.
(27) Solla-Gullon, J.; Rodes, A.; Montiel, V.; Aldaz, A.; Clavilier, J. *J. Electroanal. Chem.* **2003**, *554*, 273–284.
(28) Armand, D.; Clavilier, J. *J. Electroanal. Chem.* **1987**, *225*, 205–214.
(29) Inukai, J.; Ito, M. *J. Electroanal. Chem.* **1993**, *358*, 307.
(30) Gómez, R.; Feliu, J. M. *Electrochim. Acta* **1998**, *44*, 1191–1205.
(31) Ureta-Zanartu, M. S.; Montenegro, M.; Zagal, J. H. *Bol. Soc. Chilena Quim.* **2001**, *46*, 209–216.
(32) Choi, J. H.; Park, K. W.; Park, I. S.; Nam, W. H.; Sung, Y. E. *Electrochim. Acta* **2004**, *50*, 787–790.
(33) Williams, C. T.; Takoudis, C. G.; Weaver, M. J. *J. Phys. Chem. B* **1998**, *102*, 406–416.
(34) Dima, G. E.; de Vooys, A. C. A.; Koper, M. T. M. *J. Electroanal. Chem.* **2003**, *554−555*, 15–23.
(35) Hasnat, M. A.; Islam, M. A.; Borhanuddin, S. M.; Chowdhury, M. R. U.; Machida, M. *J. Mol. Catal. A: Chem.* **2010**, *317*, 61–67.
(36) da Cunha, M. C. P. M.; Nart, F. C. *Phys. Status Solidi A: Appl. Res.* **2001**, *187*, 25–32.
(37) Stamenkovic, V.; Mun, B. S.; Mayrhofer, K. J. J.; Ross, P. N.; Markovic, N. M.; Rossmeisl, J.; Greeley, J.; Norskov, J. K. *Angew. Chem., Int. Ed.* **2006**, *45*, 2897–2901.
(38) Stamenkovic, V. R.; Mun, B. S.; Arenz, M.; Mayrhofer, K. J. J.; Lucas, C. A.; Wang, G.; Ross, P. N.; Markovic, N. M. *Nat. Mater.* **2007**, *6*, 241–247.
(39) Strasser, P.; Koh, S.; Anniyev, T.; Greeley, J.; More, K.; Yu, C.; Liu, Z.; Kaya, S.; Nordlund, D.; Ogasawara, H.; Toney, M. F.; Nilsson, A. *Nat. Chem.* **2010**, *2*, 454–460.
(40) Schrinner, M.; Ballauff, M.; Talmon, Y.; Kauffmann, Y.; Thun, J.; Muller, M.; Breu, J. *Science* **2009**, *323*, 617–620.